Hydro-Acoustic Wave Generation during the Tohoku-Oki 2011 Earthquake

A. Abdolali[1]; James T. Kirby[2]; Giorgio Bellotti[3]; S. Grilli[4]; and J. C. Harris[5]

[1]Center for Applied Coastal Research, Univ. of Delaware, Newark DE, USA
[2]Center for Applied Coastal Research, Univ. of Delaware, Newark DE, USA
[3]Engineering Dept., Roma Tre Univ., Rome, Italy
[4]Dept. of Ocean Engineering, Univ. of Rhode Island, Narragansett, RI 02882, USA
[5]Saint-Venant Hydraulics Laboratory, Univ. Paris-Est (EDF R&D, ENPC, Cerema), Chatou, France

ABSTRACT

We investigate the surface gravity and hydro-acoustic wave fields, generated by the 2011 Tohoku-Oki tsunamigenic event using a numerical model based on a computationally efficient depth-integrated equations for a compressible water column coupled to a dissipative sedimentary layers. Spectral analysis of bottom pressure time series obtained in deep water revealed the role of underlying layer on the formation of hydro-acoustic waves and carrying frequency range, damping and trapping behaviors. The presented methodology can enhance the promptness and the accuracy of tsunami early warning systems (TEWS).

Keywords: Hydro-acoustic waves; Tsunami; Compressible Fluid; Viscous Sediment; Damping.

INTRODUCTION

Fast and tsunamigenic motions of the sea-bed, besides generating surface gravity waves, generate pressure waves in weakly compressible seawater, or hydro-acoustic waves, which propagate toward deeper water and attenuate gradually due to dissipation through sea-bottom interaction. These waves travel at the sound celerity in water, much faster than the long free-surface gravity waves in the tsunami wavetrain, and contain significant information on the source (Chierici et al., 2010). Measurement of hydro-acoustic waves can therefore anticipate tsunami arrival and significantly improve the capabilities of tsunami early warning systems (TEWS). Recent advances in deep-sea observatories have provided the opportunity to study low frequency hydro-acoustic waves. Experimental evidence of the existence of such waves generated by the seabed motion has first been found during the *Tokachi-oki* 2003 tsunami event (Nosov et al., 2007). In addition, during the Haida Gwaii 2012 earthquake, Ocean Networks Canada observatories on the southern side of the earthquake zone in British Columbia collected low frequency pressure signals using bottom pressure gauges, a few minutes after the event (Abdolali et al., 2015a). Studies, especially in the last decade, have shown that tsunami modeling can be improved by considering the compressibility of the water column, particularly during the generation stage. Up to this point, three-dimensional models were the most straightforward tools at a trackers' disposal, but, given the time constraints when dealing with tsunamis, they were found to be too time consuming. The problem was compounded by viscous sediment layers on the bottom of the sea floor, which have a strong influence on hydro-acoustic wave propagation over large distances. To address the former issue, Sammarco et al. (2013) proposed the depth-integrated Mild Slope Equation for Weakly Compressible fluid, MSEWC for a rigid bottom, which reduces the computational problem from three to two dimensions, thereby lowering computational costs. The MSEWC was subsequently applied to simulate hydro-acoustic wave

propagation in the central and eastern Mediterranean Sea, generated by two destructive historical earthquakes: the 365 AD Crete event and the 1693 Sicily event (Cecioni et al., 2014). Later, Abdolali et al. (2015a) applied the MSEWC model to reproduce the 28 October 2012 7.8 Mw earthquake, which occurred off the West coast of Haida Gwaii archipelago, Canada. The issue of bottom damping was incorporating the sediment layers' effects, which lead to a Mild Slope Equation for Dissipative Weakly Compressible fluids (MSEDWC) (Abdolali et al., 2015c). They showed that this improvement of the equations significantly improved the model's prediction. The added complexity of the sediment layer rheology leads to both the lowering of dominant spectral peaks and wave attenuation across the full spectrum. This paper presents the application of the MSEDWC to the numerical modeling of both the tsunami and hydro-acoustic waves generated by the 2011 *Tohoku-oki* earthquake. Following Tappin et al. (2014), the generation mechanism is modeled as a combination of the space and time varying co-seismic seafloor deformation caused by the earthquake followed by a submarine mass failure (SMF), triggered to the north of the main rupture after 2'15" delay. Model results are compared with field data recorded during the 2011 *Tohoku-oki* event, by the Deep-ocean Assessment and Reporting of Tsunamis (DART®) network and by the Japan Agency for Marine-Earth Science and Technology (JAMSTEC) observatories. The paper is structured as follows: Section 2 describes the 2011 *Tohoku-oki* earthquake and consequent tsunami and provides information on the instruments that recorded the event, whose data is then interpreted and used to compare to results of the numerical model. Section 3 describes the model to simulate the tsunami event a in weakly compressible fluid coupled with dissipative sedimentary layers. Discussions and conclusions are given in Section 4.

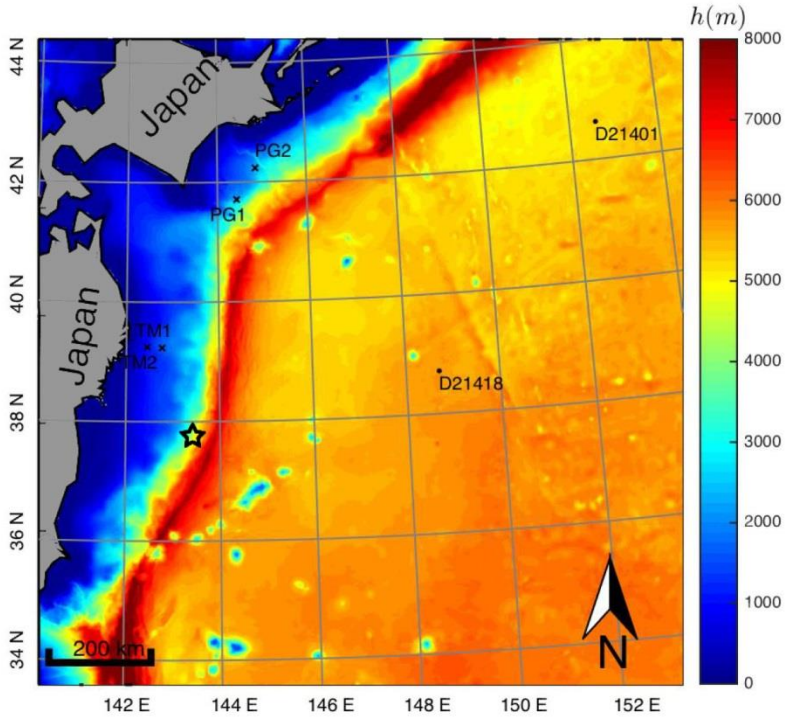

Figure 1: Bathymetry data (ETOPO1 and JAMSTEC data) with the position of bottom pressure and DART Gauges. The epicenter of 2011 *Tohoku-oki* event is shown by black star.

THE 2011 TOHOKU-OKI TSUNAMI: IN-SITU OBSERVATIONS

On March 11, 2011, at 14:46 local time (JST), a megathrust earthquake of moment magnitude *Mw* = 9.0 occurred off the *Tohoku* district, north-eastern Japan, causing a devastating tsunami that resulted in over 15,800 people's fatalities as well as over 3,300 people missing and caused enormous destruction along the coast of Japan.

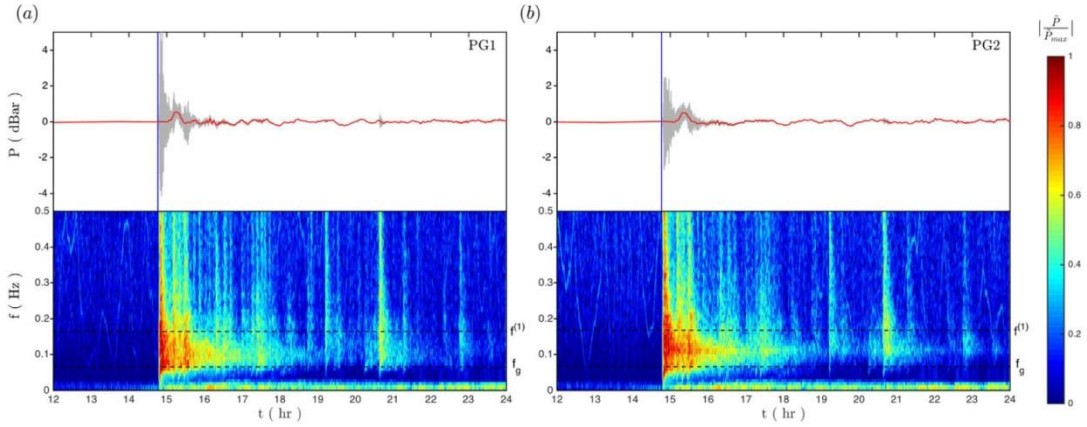

Figure 2: Upper Panels. Time series of bottom pressure recorded at PG1 (*a*) and PG2 (*b*) (Fig. 1) at 2200 m depth (detided) compare to the tsunami wave (red line) and time of main shock (14:46 JST) marked by a vertical blue line. Lower Panels. Spectrograms of bottom pressure normalized by its maximum value. The local characteristic gravitational wave frequency f_g and first acoustic mode $f^{(1)}$ are shown as horizontal dashed lines.

Bottom pressure data was collected during the event by the DART network and the Japan Agency for Marine-Earth Science and Technology (JAMSTEC) and University of Tokyo deep sea observatories. Location of observatories which recorded the waves generated by the 2011 earthquake are shown in Figure 1, together with bathy-metric information within the footprint of the numerical domain described below. The DART network was deployed by the National Oceanic and Atmospheric Administration (NOAA), to support real-time forecasting of tsunami events. The closest DART instruments that recorded the 2011 earthquake event are: DART#21418 (38° 41'17" N 148°46'9" E) in a 5662 m water depth, 500 km east of the epicenter, and DART#21401 (42°37'0" N 152°35'0" E) in a 5264 m water depth, 970 km north east of the epicenter. Tsunami warning was issued after recording strong signatures of the earthquake and then of the tsunami. The JAMSTEC cabled observatory of Hokkaido consists of three ocean-bottom seismometers (OBSs) and two ocean-bottom pressure gauges (PGs), and their datasets are sent to JAMSTEC in real-time. In this paper we consider data recorded by four submarine observatories, at *PG*1 (41°42'14" N 144°26'15"E) in a 2200 m water depth, 140 km offshore and 450 km north of the epicenter, and at *PG*2 (42°14'11" N 144°50'54"E) in a 2200 m water depth, 100 km offshore and 515 km north of the epicenter. These observatories are equipped with many instruments, including bottom pressure recorders and seismometers (*OBS* 1 and *OBS* 3). The University of Tokyo bottom pressure gauges (TMs) were located very close to the epicenter and recorded unique waveforms. These are *TM*1 (39°13'55" N 142°46'5"E) in a 1618 m water depth, 60 km offshore and 155 km north of the epicenter and *TM*2 (39°15' N 142°26'42"E) in a 1000 m water depth, 40 km offshore and 165 km north of the epicenter. The model domain is shown in Figure 1; it covers an area of about $1.44 \times 10^6 km^2$ of the Pacific

Ocean, bounded by the Japan coasts on the west side. Figure 1 shows the bathymetric data used in the numerical simulations, obtained from the National Geophysical Data Center (NGDC) database ETOPO1 and JAMSTEC. In Figure 2, the detided pressure time series recorded at JAMSTEC's bottom pressure sensors in observatories *PG*1 and *PG*2, shown in upper parts of panels (*a*) and panel (*b*), respectively, as gray lines starting from 12:00 JST. The time of the main shock (14:46 JST) is shown by vertical blue lines. Long gravitational tsunami waves are shown by red lines. The lower parts of each panel in Fig. 3 show spectrograms of bottom pressure. The local characteristic gravitational wave frequencies $f_g = \sqrt{g/h}$ and that of the first acoustic mode for a rigid bottom, $f^{(1)} = c/4h$ are shown by horizontal dashed lines (where h, c and g are water depth, sound celerity in water and gravitational acceleration, respectively). The f_g is always smaller than the minimal natural frequency $f^{(1)}$.

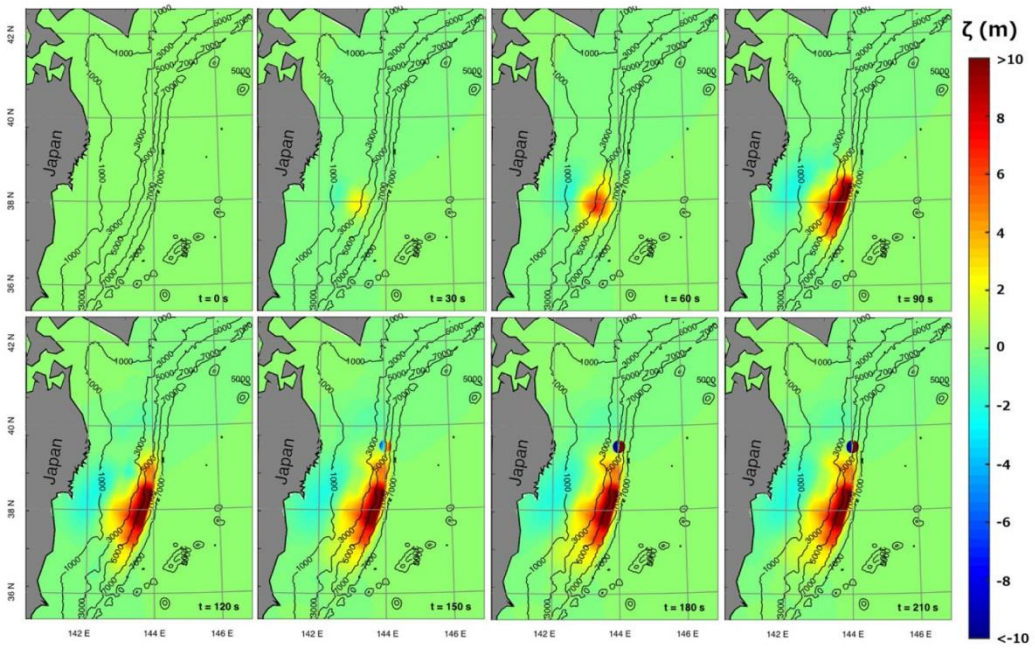

Figure 3: Time frames of seafloor deformation (color scale in meter) caused by the 2011 *Tohoku* earthquake (Grilli et al., 2013) and a dual SMF source to the north (Tap-pin et al., 2014) at 30 *s* interval. Depth range is shown by contour lines at 2000 m intervals

The reconstructed sea-bed motion is a combination of the primary vertical displacement of the seafloor due to the earthquake (Grilli et al., 2013), and an additional tsunami source consisting of a submarine mass failure triggered after 2'15" delay and lasted for 63 *s* (SMF-i.e., a submarine landslide (Tappin et al., 2014)). The earthquake caused mainly seabed uplift near the trench axis with a weaker subsidence nearshore with a maximum value of $\zeta = 11.35$ *m* in deeper part of trench. As in Tappin et al. (2014), the SMF is a rigid slump with motion idealized as a small amplitude pendulum-like motion for the slump center of mass. The simplified SMF geometry is a quasiGaussian-shaped, similar to actual slumps. More details on the generation mechanism can be found in Tappin et al. (2014). Unlike the traditional incompressible tsunami models, which often use the residual vertical displacement of the bottom as the initial free surface displacement, in this depth-integrated wave model, the spatio-temporal sea bottom motion is considered for both tsunami and hydro-acoustic modes. The snapshots of seafloor deformation shown in Fig. 3, are used as boundary condition in the numerical model.

WAVE MODEL

In the framework of hydro-acoustic wave theory, the underlying sedimentary layers can be treated as a fluid-like medium coupled with the water column at the interface (Chierici et al., 2010; Abdolali et al., 2015c). In this respect, sediment intergranular friction governs the sound propagation field, leading to changes in natural frequencies and evanescent modes of hydro-acoustic waves. Observations during the *Tokachi-oki* 2003 and the *Tohoku-oki* 2011 events show that the dominant peak frequencies are lower than values estimated by assuming a rigid bottom (see Eq.(12)), for one single water column (Nosov et al., 2007). In addition, the time series of hydro-acoustic wave amplitudes decrease exponentially (Abdolali et al., 2015b). A nondimensionalization of the sediment layer equations yields a parameter $\varepsilon = \omega \nu_s / c_s^2$ characterizing the size of the damping term relative to the undamped wave equations. For the case of a water column coupled with a sedimentary layer, the linearized compressible wave equations governing the fluid potential $\Phi(x, y, z, t)$ in the water layer and $Q(x, y, z, t)$ in the stratified viscous sediment layer, and the boundary conditions at the free surface and at the bottom, are given by

$$\begin{cases} \Phi_{tt} - c^2 \nabla^2 \Phi = 0; & -h + \eta_2 \le z \le \eta_1 \\ Q_{tt} - c_s^2 \nabla^2 Q - 2\nu_s (\nabla^2 Q_t) = 0; & -h_s \le z \le -h + \eta_2 \\ \Phi_{tt} + g\Phi_z = 0; & \text{at } z = 0 \\ Q_z + \nabla_h h_s \cdot \nabla_h Q + h_{s,t} = 0; & \text{at } z = -h_s \end{cases} \tag{1}$$

where ∇^2 is the Laplacian in 3D and subscripts on dependent variables denote partial derivatives. ∇_h is the horizontal gradient operator and $h_{s,t}$ is the vertical bottom velocity representing displacement of the impermeable substrate. The interfacial displacements $\eta_i(x, y, t)$; $i = 1, 2$, represent the response of the free surface and interface to hydro-acoustic disturbances. The apparent sediment kinematic viscosity is $\nu_s = \mu_s/\rho_s$. The bulk viscosity μ_s ranges from 10^6 up to 10^{20} Pa s (Van Keken et al., 1993). Matching conditions at the water-sediment $z = -h + \eta_2$ consist of continuity of pressure and kinematic constraints for each layer.

MILD SLOPE EQUATION FOR DISSIPATIVE WEAKLY COMPRESSIBLE FLUIDS (MSEDWC)

Considering a single underlying sedimentary layer, $h_s = h + a$, in the hypothesis of constant sound c and c_s, the upper and lower layer potentials may be expressed as $\Phi(x, y, z, t) = \sum_{n=0}^{\infty} \psi_n(x, y, t) M_n(z)$ and $Q(x, y, z, t) = \sum_{n=0}^{\infty} \psi_n(x, y, t) N_n(z)$ respectively. The eigenfunctions $M_n(z)$ and $N_n(z)$ for the upper and lower layers are given by

$$M_n = \frac{(1 - \lambda_n \mathrm{T}_n)\cosh(\beta_{w,n}(h+z)) + (\lambda_n - \mathrm{T}_n)\sinh(\beta_{w,n}(h+z))}{(1 - \lambda_n \mathrm{T}_n)\cosh(\beta_{w,n}h) + (\lambda_n - \mathrm{T}_n)\sinh(\beta_{w,n}h)} \tag{2}$$

$$N_n = \frac{(\lambda_n - \mathrm{T}_n)\cosh \beta_{s,n}(h_s + z)}{\alpha_n \sinh(\beta_{s,n}a)[(1 - \lambda_n \mathrm{T}_n)\cosh(\beta_{w,n}h) + (\lambda_n - \mathrm{T}_n)\sinh(\beta_{w,n}h)]} \tag{3}$$

where $\mathrm{T}_n = \tanh(\beta_{w,n}h)$, $\lambda_n = \omega^2/g\beta_{w,n}$ and $\alpha_n = \beta_{s,n}/\beta_{w,n}$. The separation constants $\beta_{w,n}$ and $\beta_{s,n}$ for water and sediment layers respectively are given by

$$\beta_{w,n}^2 = k_n^2 - \left(\frac{\omega}{c}\right)^2; \quad \beta_{s,n}^2 = k_n^2 - \left(\frac{\omega}{c_s}\right)^2 \tag{4}$$

where k_n is the wave number. The dispersion relation for $\beta_{w,n}$ and $\beta_{s,n}$ is given by

$$\lambda_n^2(R+\alpha_n \mathrm{T}_n\hat{\mathrm{T}}_n)-\lambda_n R(\mathrm{T}_n+\alpha_n\hat{\mathrm{T}}_n)+(R-1)\alpha_n\mathrm{T}_n\hat{\mathrm{T}}_n=0 \tag{5}$$

where $R = \rho_s/\rho$ and $\hat{\mathrm{T}}_n = \tanh(\beta_{s,n}a)$. Eq. (5) is a quartic system in ω describing a doubly-infinite set of surface waves (with horizontal displacements in phase at the layer interface) and internal waves (with horizontal displacements 180° out of phase). By a proper use of the averaging technique to problem (1), taking advantage of the orthogonality within the spatial derivative terms, and making use of the interfacial kinematic and dynamic boundary conditions, Abdolali et al. (2015c) found a hyperbolic mild slope equation (MSEDWC) for weakly compressible fluid overlying a sediment viscous layer, in the following form

$$\left(I_2^m\psi_{m,t}\right)_t-\nabla_h\cdot[I_1^m\nabla_h\psi_m]+[\omega^2 I_2^m-k_m^2 I_1^m]\psi_m+2R\varepsilon\frac{\omega}{c_s^2}K_n\psi_{m,t}=D_1^m h_t+D_2^m h_{s,t}, \tag{6}$$

Model coefficients are given by

$$I_1^m=I_{mm}+RK_{mm};\quad I_2^m=\frac{I_{mm}}{c^2}+R\frac{K_{mm}}{c_s^2}+\frac{1}{g} \tag{7}$$

$$D_1^m=-[M_m(-h)-RN_m(-h)];\quad D_2^m=-RN_m(-h_s), \tag{8}$$

where $I_{mm}(x, y, t)$, $K_{mm}(x, y, t)$, G_1^m and G_2^m are given by

$$I_{mm}=\int_{-h}^{0}M_m^2dz=\frac{h}{2G_1^m}[(1-2\lambda_m\mathrm{T}_m+\lambda_m^2)+(1-\lambda_m^2)G_1^m] \tag{9}$$

$$K_{mm}=\int_{-h_s}^{-h}N_m^2dz=\frac{h\left(\lambda_m-\mathrm{T}_m\right)^2}{2\alpha_m^3\mathrm{T}_m\hat{\mathrm{T}}_m}\frac{1+\mathrm{G}_2^m}{\mathrm{G}_1^m} \tag{10}$$

$$\mathrm{G}_1^m=\frac{2\beta_{w,m}h}{\sinh(2\beta_{w,m}h)};\quad \mathrm{G}_2^m=\frac{2\beta_{s,m}a}{\sinh(2\beta_{s,m}a)} \tag{11}$$

More details on the derivation can be found in Abdolali et al. (2015c).

HYDRO-ACOUSTIC WAVES

The superposition of the solutions of equation (6) for each mode leads to a complete modeling of the fluid potential generated by a fast sea-bed motion. Since the water depth in the generation area dominates the frequency spectrum, where the majority of wave energy is concentrated, we define the frequency range and the number of hydro-acoustic modes to solve for, in order to minimize the computational cost while maintaining good accuracy. In the absence of viscous behavior of the sea bottom, the dominant frequency range in the wave spectrum can be expressed by a discrete set of normal frequencies $f^{(n)}$ given by

$$f^{(n)}=(2n-1)\frac{c}{4h},\quad n=1,2,3,\cdots \tag{12}$$

As it has been shown by contour lines in Figure 3, the depth in the generation zone varies between 2000 and 7000 *m*. Therefore, the dominant frequency range for the case of rigid bottom is $f^{(1)}$ =0.054 − 0.1875 Hz. Introducing a single underlying sediment layer acting together with the water column lowers the spectral peak frequencies, which are solution of the following transcendental equation (Nosov et al., 2007):

$$\tan[\frac{2\pi\gamma^{(n)}h}{c}]\tan[\frac{2\pi\gamma^{(n)}a}{c_s}]=\frac{\rho_s c_s}{\rho c} \quad (13)$$

where $\gamma^{(n)}$ denotes the normal mode frequencies for the coupled case. Hence, in the case of a = 1000 m, the dominant frequency range for the case of viscous bottom $\gamma^{(1)}$ =0.051 − 0.161 Hz. It has been shown that the 1^{st} mode carries most of the hydro-acoustic wave energy, and the solution of the selected frequency range reproduces accurately the main wave features (Abdolali et al., 2015a; Cecioni et al., 2014). The modeling of hydro-acoustic waves has been carried out by solving equation (6) for $n \geq 1$ and for a number of frequencies within the finite range f = 0.04 - 0.2 Hz. As has been discussed, the solution within this range enables us to optimize the computations. In order to correctly reproduce the hydro-acoustic wave field in the numerical domain of Figure 1, a maximum grid size of 1 km was selected, for a total number of 3,000,000 triangular elements. The solutions computed on a high-speed computer equipped with 12 cores i7 3.20 GHz CPU and 64GB RAM. The MUMPS solver (MUltifrontal Massively Parallel sparse direct Solver) was used. The computations were done for solving 800 s. Due to the uncertainties about complicated characteristics of sedimentary layer, we first investigated the generation and propagation of hydro-acoustic waves in the absence of damping in the sea bottom, to reveal the propagation path and behavior of acoustic waves in real applications. Results of this large scale simulation for the case of couple layers with μ = 0 are shown in Figure 4 in terms of bottom pressure, $P(x, y, t)$. We see that a complicated perturbation pattern is formed, which propagates at the sound celerity in water. Acoustic waves reach the domain offshore boundaries12 minutes after the event. Figure 4 also shows that hydro-acoustic waves do not propagate upslope; but get trapped within the deep trench at the edge of the continental shelf and spread laterally. This unique response to the Japan trench geometry was not observed for the Haida Gwaii 2012 event where simulations showed the propagation of acoustic waves perpendicular to the fault orientation (Abdolali et al., 2015a). The present results illustrate the significant effect of the bathymetry on hydro-acoustic wave propagation.

In another simulation, the kinematic viscosity in the viscous sediment layer, μ, was considered, in order to see the damping behavior included by the sea bottom on the hydro-acoustic wave field. The damping coefficient was inferred from the analysis of bottom pressure time series collected during the *Tokachi-oki* 2003 and later the *Tohoku-oki* 2011 done by Chierici et al. (2010) and Abdolali et al. (2015b). Results of numerical simulations are shown in Figure 5, in terms of maximum absolute bottom pressure normalized by its maximum value, for the case of μ = 0 in panel (*a*) and $\mu = 2 \times 10^{10}$ *Pa.s* in panel (*b*). From panel (*a*), the propagation path of hydro-acoustic waves towards deeper water can be interpreted: as waves propagate farther, their energy spreads and their intensity decreases. The scattered sea-mounts restrict passage of the lower frequencies. The observations and simulations prove that hydro-acoustic waves can reach shallower areas than when assuming bottom, due to the increase in depth caused by adding the lower layer and tunneling effects. As was shown in panel (*b*), the hydro-acoustic waves are mainly localized in the generation area. These results indicate the significant role of dissipation in sea bottom. In addition, it can be concluded that regardless of damping in the sea bottom, fluid compressibility should be considered in the generation area.

TSUNAMI WAVES

Numerical simulations of long surface gravity waves generated by the 2011 *Tohoku-oki* event was performed by solving for the zero-th mode of equation (6). Equation (6) is solved by means

of a Finite Element Method on the numerical domain of Fig. 1, which has been discretized in triangular elements, here with a maximum size of 3 km. There are 1,500,000 grids for the model. The computations were done for simulation of 90 minutes of real time. Frequencies in the range f = 0 - 0.03 Hz, with a df = 0.002 Hz, were solved to reconstruct the gravitational wave field. Results of the tsunami model are shown in Figure 6, in terms of bottom pressure time series at the JAMSTEC observatories, *PG*1, panel *a* and *PG*2, panel *b*; *TM*1, panel *c* and *TM*2, panel *d*; and at the DART buoys *DART*#21401, panel *e* and *DART*#21418, panel *f*, respectively. The black lines show results of the numerical model, while the blue lines represent the pressure signals recorded at the instruments. The comparison between the model and the field data at the observatories shows a good agreement in terms of amplitude, period and arrival time of the pressure signal given by the long gravity wave transit. Both numerical and field data reveal that tsunami waves arrived at the *DART*#21401 and *DART*#21418 buoys, 55 and 28 minutes after the event. Although the sampling frequency of DART records is not sufficient to resolve the fast elastic oscillations and low-frequency hydro-acoustic waves (0.066 Hz), there are some perturbations a few minutes after the earthquake. The field pressure data, however, includes the pressure variation given by the ground motion and the precursor waves.

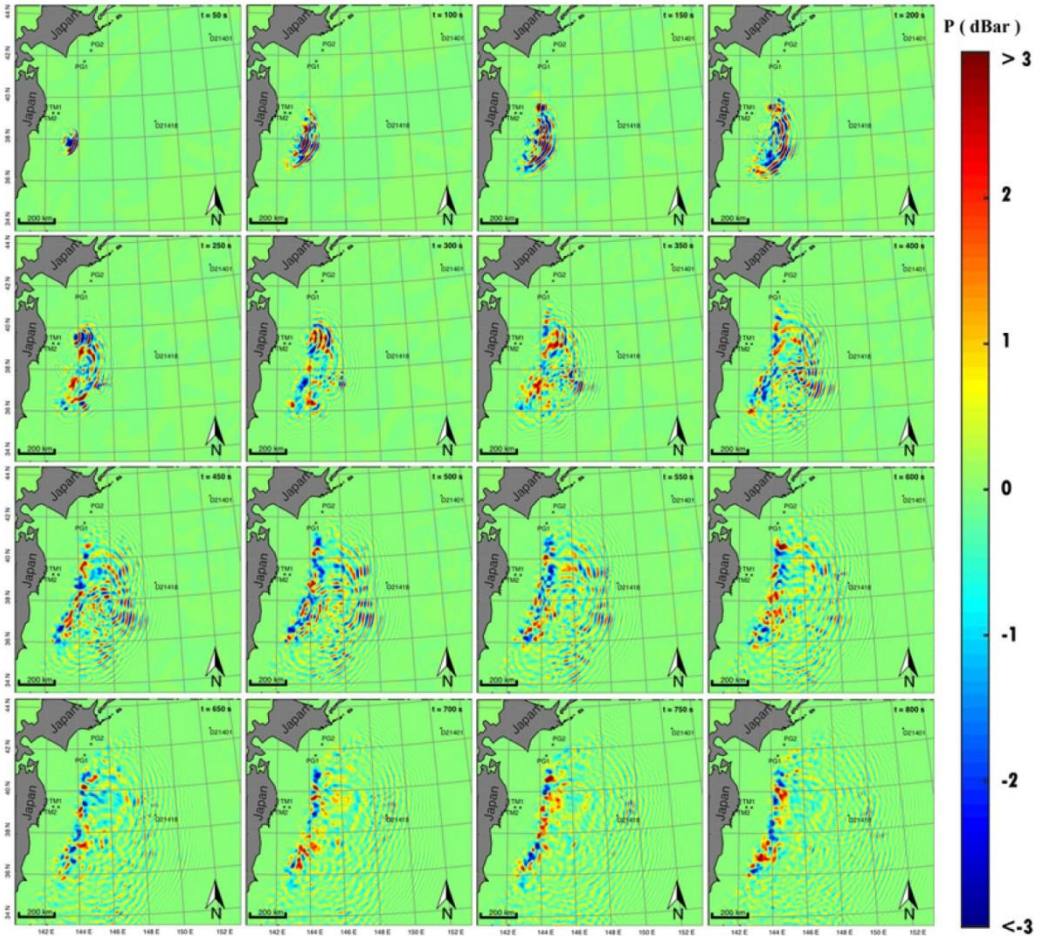

Figure 4: Snapshots of the bottom pressure (*P*) hydro-acoustic wave perturbation generated by the 2011 *Tohoku-oki* earthquake and SMF. *t* = 0 refers to the time of occurrence of the earthquake.

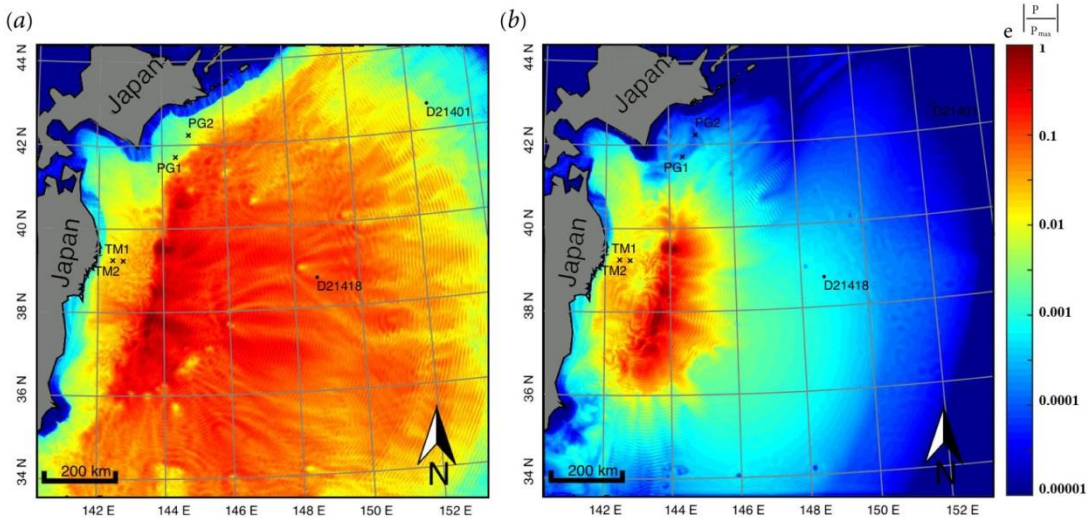

Figure 5: Maximum absolute values of the computed bottom pressure from hydro-acoustic waves normalized by its maximum value, generated by the 2011 *Tohoku-oki* earthquake and SMF. (*a*) $\mu = 0$; (*b*) $\mu = 2 \times 10^{10}$ *Pa.s*.

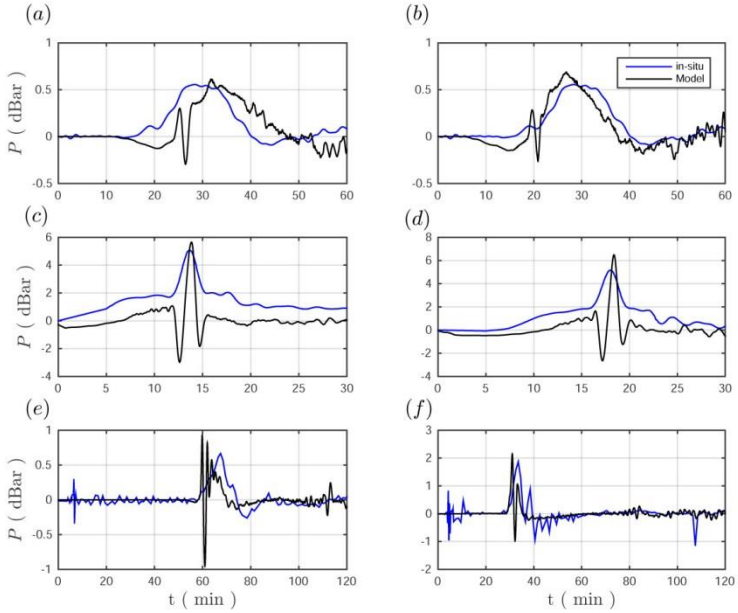

Figure 6: Time series of free surface elevation (η) at (*a*) PG1; (*b*) PG2; (*c*) TM1; (*d*) TM2; (*e*) DART#21401 and (*f*) DART#21418: measured (blue lines), and calculated by the hydro-acoustic model for gravity wave (black lines). $t = 0$ refers to the time of occurrence of the earthquake.

Figure 7 depicts the time history of generation and propagation of tsunami waves in the computational domain. The plot shows that the residual bottom dislocation is almost transferred to the sea surface. The wave front starts spreading and covers the entire domain after 90 minutes. Comparison between Figures 4 and 7 shows that, except for the initial stages of the generation process, the significant difference between the speed of low-frequency and tsunami waves leads to the different location of hydro-acoustic and tsunami wave fronts in time.

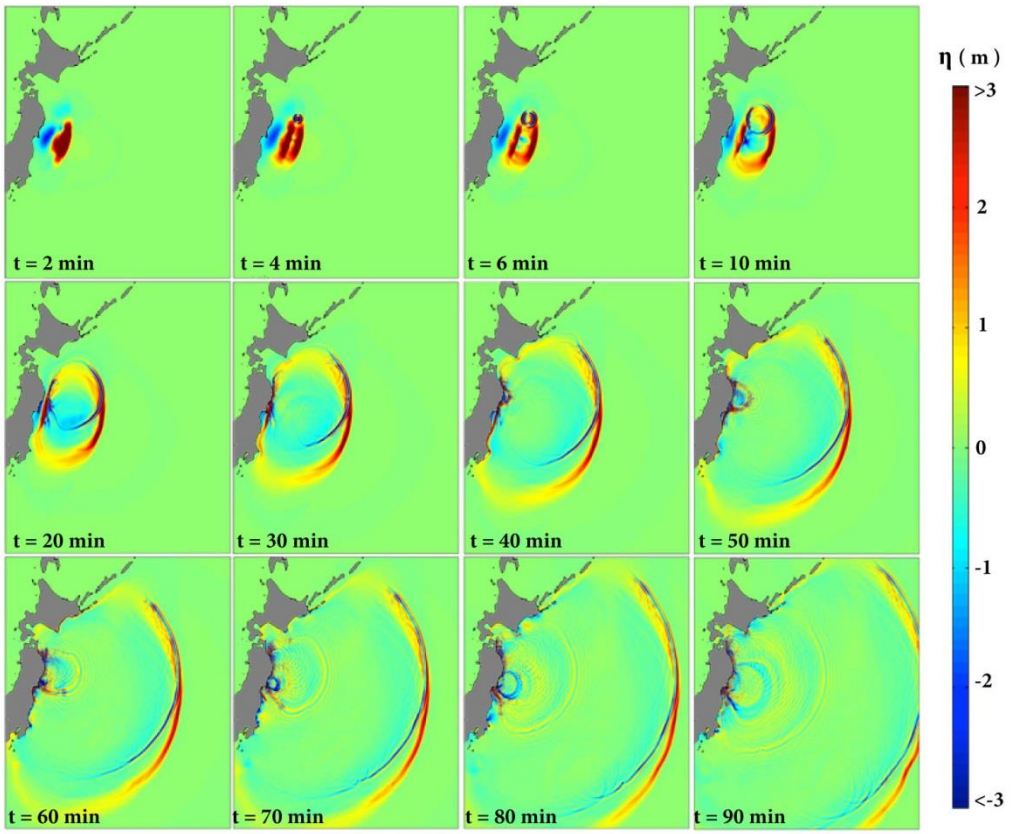

Figure 7: Snapshots of surface (η) gravity wave elevation generated by the 2011 *Tohoku-oki* earthquake and SMF, computed qith the hydro-acoustic model. t = 0 refers to the time of occurrence of the earthquake.

CONCLUSION

Here we show a first application of a model based on the Mild Slope Equation for Dissipative Weakly Compressible fluids, MSEDWC, to simulate the pressure and surface waves generation, propagation and attenuation during the 2011 *Tohoku-oki* tsunami-genic event in a large scale domain, overcoming the computational difficulties of three-dimensional models. Since the devastating coastal impact of the 2011 *Tohoku-oki* tsunami could not be fully explained from a co-seismic source alone, a combination of a coseismic source and a submarine mass failure (SMF) was used as a dual tsunamigenic source, in order to improve model results with observations. The model outputs can be used for diagnosis of generation mechanism and sediment structure in respond to hydro-acoustic waves. The comparison was done in order to understand the effects of sea bottom geometry on low-frequency hydro-acoustic waves propagation and attenuation patterns to be able to better use and integrate deep sea observatories as a part of Tsunami Early Warning Systems (TEWS).

ACKNOWLEDGMENTS

The authors acknowledge the support of the National Tsunami Hazard Mitigation Program, NOAA, grants NA14NWS4670041 and NA15NWS4670029 and the NSF ENH program, grant CMMI-1537232.

REFERENCES

Abdolali, A., Cecioni, C., Bellotti, G., and Kirby, J. T. (2015a). Hydro-acoustic and tsunami waves generated by the 2012 Haida Gwaii earthquake: Modeling and in situ measurements. *Journal of Geophysical Research: Oceans*, 120(2169-9291).

Abdolali, A., Cecioni, C., Kirby, J. T., Sammarco, P., Bellotti, G., and Franco, L. (2015b). Numerical modeling of low frequency hydro-acoustic waves generated by submarine tsunamigenic earthquake. In *Proceedings of the Twenty-fifth (2015) International Ocean and Polar Engineering*, volume 3, pages 725–732.

Abdolali, A., Kirby, J. T., and Bellotti, G. (2015c). Depth-integrated equation for hydro-acoustic waves with bottom damping. *Journal of Fluid Mechanics*, 766, R1.

Cecioni, C., Abdolali, A., Bellotti, G., and Sammarco, P. (2014). Large-scale numerical modeling of hydro-acoustic waves generated by tsunamigenic earthquakes. *Natural Hazards and Earth System Sciences Discussions*, 2(7):4629–4658.

Chierici, F., Pignagnoli, L., and Embriaco, D. (2010). Modeling of the hydroacoustic signal and tsunami wave generated by seafloor motion including a porous seabed. *Journal of Geophysical Research*, 115(C03015).

Grilli, S., Harris, J., Tajalli Bakhsh, T., Masterlark, T., Kyriakopoulos, C., Kirby, J., and Shi, F. (2013). Numerical simulation of the 2011 Tohoku tsunami based on a new transient fem co-seismic source: Comparison to far- and near-field observations. *Pure and Applied Geophysics*, 170(6-8):1333–1359.

Nosov, M., Kolesov, S., Denisova, A., Alekseev, A., and Levin, B. (2007). On the near-bottom pressure variations in the region of the 2003 Tokachi-oki tsunami source. *Oceanology*, 47(1):26–32.

Sammarco, P., Cecioni, C., Bellotti, G., and Abdolali, A. (2013). Depth-integrated equation for large-scale modelling of low-frequency hydroacoustic waves. *Journal of Fluid Mechanics*, 722:R6.

Tappin, D. R., Grilli, S. T., Harris, J. C., Geller, R. J., Masterlark, T., Kirby, J. T., Shi, F., Ma, G., Thingbaijam, K., and Mai, P. M. (2014). Did a submarine landslide contribute to the 2011 Tohoku tsunami? *Marine Geology*, 357:344 – 361.

Van Keken, P., Spiers, C., Van den Berg, A., and Muyzert, E. (1993). The effective viscosity of rocksalt: implementation of steady-state creep laws in numerical models of salt diapirism. *Tectonophysics*, 225(4):457–476.